RSC Advances

ROYAL SOCIETY OF CHEMISTRY

www.rsc.org/advances

Cite this: DOI: 10.1039/c0xx00000x

www.rsc.org/xxxxxx

ARTICLE TYPE

An Efficient Thermoelectric Material: Preparation of Reduced Graphene Oxide/Polyaniline Hybrid composites by Cryogenic Grinding

Weijie Wang[a], Qihao Zhang[a], Jianlin Li[b], Xia Liu[a], Lianjun Wang*[a], Juanjuan Zhu[a], Wei Luo[a], Wan Jiang*[a,c]

[a]State Key Laboratory for Modification of Chemical Fibers and Polymer Materials, Donghua University, Shanghai 201620, People's Republic of China

[b] Key Laboratory of Ministry of Education for Advanced Materials in Tropical Island Resources, School of Materials and Chemical Engineering, Hainan University, 58 Renming Ave, Haikou 570228, China

[c]School of Material Science and Engineering, Jingdezhen Ceramic Institute, Jingdezhen 333000, China

Received (in XXX, XXX) Xth XXXXXXXXX 20XX, Accepted Xth XXXXXXXXX 20XX

DOI: 10.1039/b000000x

An alternative and facile strategy to fabricate conducting reduced graphene oxide/polyaniline (RGO/PANI) hybrid composites with highly enhanced thermoelectric properties is introduced. RGO and PANI were homogeneously mixed by cryogenic grinding and then consolidated via Spark Plasma Sintering. X-ray diffraction, X-ray photoelectron spectroscopy, Fourier transform infrared spectroscopy and Transmission electron microscope are employed to evaluate the phase structure and microstructure of the as-prepared composites. The results show that CG technique could not only effectively refine the grain size of PANI, but also induce more dislocations. The refined PANI particles are homogeneously dispersed and orderly arranged on the rGO templates thanks to the strong π-π conjugated interactions between PANI and rGO. The thermoelectric properties of the PANI samples containing different rGO content are systematically investigated. Compared with pure bulk PANI, rGO/PANI hybrid composites exhibit a distinct enhancement in the thermoelectric performance. Both the Seebeck coefficient and the electric conductivity are found to increase remarkably resulting from the increased carrier mobility. The maximum Seebeck coefficient and electric conductivity of the rGO/PANI hybrid composites amazingly reach 15.934 μV/K and 1858.775 S/m, respectively, and the maximum ZT is up to 4.23×10^{-4}.

Introduction

Searching and developing new, clean, effective and reproducible energy has become one of the most critical issues. Thermoelectric (TE) material could achieve the mutual conversion between thermal energy and electric energy, which has received renewed attention due to its great potential for applications in Peltier coolers and thermoelectric power generators.[1,2] As is known, the performance of thermoelectric material is determined by its dimensionless figure of merit ZT ($ZT=S^2\sigma T\kappa^{-1}$, where S, σ, κ and T are the Seebeck coefficient, electrical resistivity, thermal conductivity and absolute temperature, respectively.). It's obvious that a high ZT should possess high σ, large S and low κ. Over the past half century, how to enhance ZT over 1 for practical use has become a research hotspot.[3] Until now, the performance research of TE materials have mainly focused on inorganic semiconductors, such as PbTe, Bi_2Te_3, $CoSb_3$, SnSe and theirs alloys or composites.[4-8] Compared with inorganic thermoelectric materials, conducting polymers thermoelectric materials (such as poly(3,4-ethylenedioxythiophene)[9], polyaniline[10], Polypyrrole[11]) have intrinsically low thermal conductivity, low toxicity, mechanical flexibility and inexpensive possibility, which have been widely considered as a potential candidate for TE materials[12]. Particularly, due to the low cost, structural diversification, unique doping/dedoping progress, low thermal conductivity, and the nature of easy to synthesis, PANI is regarded as one of the most potential effective and suitable TE materials among conducting polymers[13]. However, the power factor ($S^2\sigma$) for PANI thermoelectric materials is in the range of 10^{-6}-10^{-10} $Wm^{-1}K^{-2}$, which leads to the serious lag of its large-scale application.[14] In the last decade, carbon materials have been introduced into the PANI matrix to enhance its thermoelectric properties, such as graphite oxide, CNTs and graphene.[15-18]

Graphene, as a new form of carbon, has attracted great interest because of its intriguing two-dimensional sheet of sp2-bonded, 3 single-atom-thick graphene. In addition to the thinness, mechanical strength and material flexibility, graphene , a single layer of carbon atoms arranged in a hexagonal honeycomb lattice, has some outstanding physical properties such as high carrier mobility (in excess of 10^5 cm^2/Vs) and high thermal conductivity (up to 5000W/mK).[19,20] Because of these excellent performance, a much wider application of these materials and composites materials, especially for graphene composites with polyaniline is possible, such as resonators, catalyst supports, electronic devices, supercapacitors, batteries, solar cell.[21-27] The strong π-π interaction between the graphene structure and aromatic rings of polyaniline would facilitate electron delocalization and improve the electrical conductivity of the composites.[28] Nevertheless, several of these applications are still not feasible because the large-scale production of pure grapheme sheets remains challenging. The chemical reduction of graphite oxide (GO) is one of the established procedures to make graphene in large

volume.[29] Many primary products with high conductivity but poor solubility have been made by chemical reduction. However, the lower content of oxygenic groups on the surface of rGO often results in severe aggregation and agglomeration. In order to improve the dispersibility of rGO in composites, some progress has been made by using surfactants.[30] For example, Zhang K. et al. prepared chemically modified graphene and polyaniline fiber composites by in situ polymerization of aniline monomer in the presence of graphene oxide under acid conditions and then using hydrazine to reduce.[31] Kumar NA. et al. prepared graphene oxide/polyaniline with a mild oxidant by in situ polymerization.[32] Graphene ultrasonic treated with a mixture of aniline monomer and ammonium persulfate to form PANI on its surface by Al-Mashat L. and his colleagues.[33] But the methods all above are complex and time-consuming. So, it is necessary to find a simple, low-cost and environmentally friendly way to prepare rGO/PANI composites.

In this work, we report a novel and green method for fabricating nanostructured rGO/PANI composites. As-synthesized rGO/PANI composite powder are prepared using cryogenic grinding (CG) without any dispersant.[34] After the CG process, the grain size of PANI has been refined and rGO sheets are also uniformly dispersed in the composites. Meanwhile, PANI well-alignedly disperses on the rGO template because of the strong π-π conjugated interactions between PANI and rGO. Finally, the composites powers were consolidated via Spark Plasma Sintering (SPS). With the rGO template, carrier transports are improved between the interchain and intrachain of PANI following the variable range hopping.[35] An ordered chain arrangement reduce barrier of both interchain hopping and intrachain hopping and enhance the carrier mobility.[36] Moreover, it has been found rGO has extraordinary electrical conductivity, which becomes effective conductive medium for carrier transmission in rGO/PANI composites. Therefore, the electrical conductivity and power factor of composites are found to increase with the rGO adding.

Materials Synthesis

1. Preparation of PANI

Aniline (99.9%, monomer) and ammonium peroxydisulfate (APS, initiator) come from Sinopharm Chemical Reagent Co., Ltd. Particularly, the aniline cannot come into use until it is distill-purified. Corresponding solutions were prepared using deionized water during the synthesis process.

In a typical synthesis of PANI, solution A: 10ml of aniline was diluted with 200ml of 1M HCl. Then, 20g of $(NH_4)S_2O_8$ dissolved in 200ml of 1M HCl were slowly added into the solution A under stirring to form a brown slurry. The polymerization reaction was carried out for 5h at 0℃. The mixture was filtered, washed with deionized water for three times, and finally dried at 60℃ in a vacuum oven.

2.Preparation of reduced graphene oxide

Synthesis of GO: GO was prepared according to the modified hummers method reported elsewhere.[37] 1g of purified natural graphite powder was added to a flask and filled with concentrated cold H_2SO_4 (25 ml) at 0 °C, followed by addition of $KMnO_4$ (3.5 g) gradually at 0 °C (ice bath). After slowly increasing temperature to 40 °C, the mixture was stirred for 2h. Water (200 ml) was added at least three times into the mixture and then H_2O_2 (30 wt% 5 ml) was added at least three times to react with excess $KMnO_4$. The as-prepared GO precipitated quickly after 3 hours because of the strong acid environment. The precipitate mixture was washed with HCl solution (1M 1 L) by for 5 times. Then water (1L) was added to the mixture. Finally, the colloid was centrifuged at 8000 rpm for 60 min to remove graphite and large GO flakes. The obtained GO colloid used to prepare all the composite samples.

The reduced graphene oxide was prepared according to the method of Gao et al.[38] The GO colloid was dispersed in water to give a 1.0g/l colloidal solution. 5 wt% sodium carbonate solution was used to adjust the PH of the solution to 9~10. 1600mg Sodium borohydride was directly added into 200 ml GO dispersion under magnetic stirring for 30 minutes, and the mixture was kept at 90 °C for 1 h with constant stirring. Then product was filtered and washed with plenty of water for several times. This partially reduced GO was redispersed in concentrated sulfuric acid and heated to 120 °C (oil bath) with stirring for 12 h. After cooling down, the dispersion was added with large volume of deionized water. The final product was thoroughly rinsed with water. The product powder was further annealed at 1100 °C under gas flow of Ar with15 vol% H_2 for 15 minutes.

3. Preparation of rGO/PANI composites

For the rGO/PANI composites, the samples were fabricated through cryogenic grinding by a CG machine (SPEX SamplePrep 6770 Freezer/Mill, TECH-Knowledge International co., California, USA). The sample, plugs and impactor were embedded in a granding vial, and then the vial was precooled in liquid nitrogen to make the sample brittle. 1g polyaniline was grinded at -195.6 °C in the liquid nitrogen for 40min, then the sample containing polyaniline and different mass fractions (0, 5%, 10%, 20%, 30%) of rGO was grinded at -195.6 °C for 40min. Finally, the as-milled composite powders was consolidated at 100 °C for 10 min by a spark plasma sintering (SPS, Dr. Sinter 725; Sumitomo Coal Mining Co., Tokyo, Japan).

Characterization

Power X-ray diffraction (PXRD) measurement was performed using a diffractometer (D/Max-2550PC) with Cu Kα (λ=0.15406nm) radiation. The structures of composite samples were measured by a Nicolet 8700 FTIR spectrometer. The spectra were collected by the averaging of 32 scans ranging from 500 to 4000 cm^{-1}. The morphology of rGO was observed by transmission electron microscopy (TEM, Model 2100F, Japan) with a selected area electron diffraction (SAED). Raman spectra were collected using an Avalon Instruments Raman Station with a 532 nm He–Ne laser. X-ray photoelectron spectroscopy (XPS) was performed on a PHI Quantera SXM Scanning X-ray Microprobe with an Al cathode (hv=1486.6 eV) as the X-ray source set at 100 W and a pass energy of 26.00 eV. For the thermoelectric properties, the resistivity and Seebeck coefficient were investigated by Seebeck Coefficient/Electric Conductivity Measuring System (ZEM-3). The thermal diffusivity was investigated by a laser-flash method on a disk using a commercial system (LFA427; Netzsch Instruments, Selb, Germany). The Hall coefficient RH measurement of the sample was carried out on a PPMS system (Quantum Design INC., USA) with a magnetic field of 2 T and an electrical current of 30 mA.

Morphology characterization

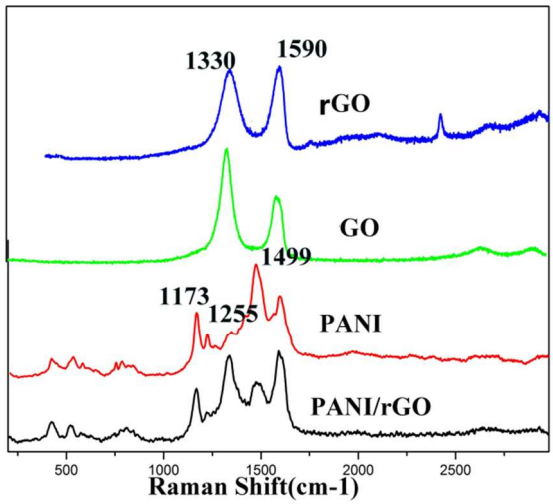

Fig.1 Raman spectra for rGO, GO and CGed-PANI/(5wt%)rGO

As shown in Figure 1, significant structural changes occur during the chemical processing from GO to rGO. PANI and the formation of PANI/rGO composites are reflected in the Raman spectra. As expected, the Raman scattering of the as-prepared GO and rGO display two prominent Raman-active peaks at 1330 and 1590 cm^{-1}, which correspond to the well-documented D mode of a sp2-hybridized carbon and the G mode related to the vibration of a sp3, hybridized carbon, respectively.[32,39-41] It is worth noting that the intensity ratio of D and G bands has been widely used as an indicator of the amount of disorders. Meanwhile, we can observe that GO has a lower I_D/I_G compared to rGO, which indicates that GO have been successful reduced. For PANI sample, the C-H bending of quinoid ring at 1173 cm^{-1}, the C-H bending of the benzenoid ring at 1255 cm^{-1}, C-N+ stretching at 1344 cm^{-1}, and C-C stretching of the benzene ring at 1499$cm^{-1}$are obviously observed, respectively. For PANI/rGO composites, the reduced intensities of two peaks (D band and G band) in the spectra of PANI/rGO at 1330 and 1590 cm^{-1} are probably due to the strong interactions between PANI and rGO.[42] Therefore, the evidences of Raman demonstrate that the PANI has dispersed on the rGO sheets.

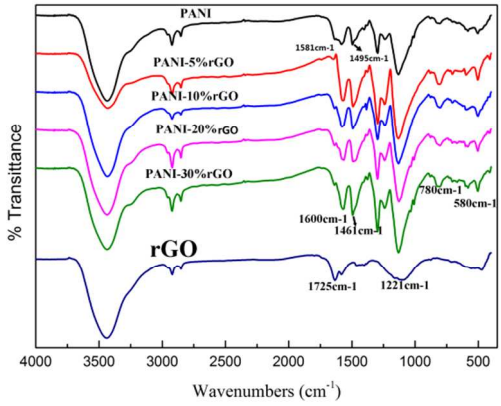

Fig.2 FTIR spectra of rGO, CGed-PANI, PANI, CGed-PANI/(5wt%)rGO, CGed-PANI/(10wt%)rGO, CGed-PANI/(20wt%)rGO, and CGed-PANI/(30wt%)rGO

The FTIR spectra for the rGO, pure PANI and PANI/rGO composites with the increasing of rGO content from 5% to 30% are shown in Fig.2. As is commonly observed for PANI, the quinoid band is less intense than the benzenoid band. The peaks at 804 cm^{-1}, 1130 cm^{-1}, 1397 cm^{-1}, 1638 cm^{-1} and 3435 cm^{-1} can be assigned to the C-H out-of-plane bending vibration, C=N stretching (-N=quinoid=N-) vibration, C-N stretching vibration in aromatic, C=O stretching vibration, and N-H stretching mode, respectively.[43,44] RGO shows the presence of strong bands at around 1636 and 1109 cm^{-1}, characteristic of C=C and C-C, respectively, associated with the stretching modes of the ester linkage.[45] Several new peaks attributed to PANI appear in the spectrum of PANI/rGO. Notably, many low-intensity peaks ranging from 580 to 780 cm^{-1} can be assigned to the vibrations of the C-H bonds in the benzene rings. While the band at about 800 cm^{-1} could be attributed to the C-H out-of-plane bending vibrations. In addition, a stretching band assigned to C-N also appears at 1300 cm^{-1}.[46] The appearance of the quinonoid and benzenoid ring vibrations (C=C stretching deformations) at about 1564 and 1461 cm^{-1}, respectively, clearly indicates the presence and formation of PANI on the graphene surfaces. As is commonly observed, the quinonoid band at 1564 cm^{-1} is less intense than the benzenoid band at 1461 cm^{-1}.[47] The characteristic band attributable to the N-Q-N-Q stretch of the quinonoid ring is also found at around 1144 cm^{-1}, which clearly supports our hypothesis that the PANI has been covalently dispersed onto the surface of the rGO sheets because of the strong π–π conjugation interaction.[48]

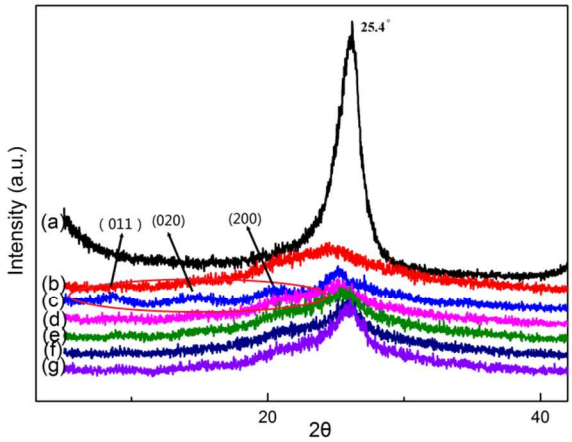

Fig.3 X-ray diffraction of (a) rGO, (b) CGed-PANI, (c) PANI, (d) CGed-PANI/(5wt.%)rGO, (e) CGed-PANI/(10wt.%)rGO, (f) CGed-PANI/(20wt.%)rGO, (g) CGed-PANI/(30wt.%)rGO.

Fig.3 shows the X-ray diffraction pattern for rGO, PANI, CGed-PANI and CGed-PANI/rGO composites. The XRD peaks from PANI are observed at 2θ=14.92°, 20.74° and 25.28°, corresponding to (011), (020) and (200), reflection of polyaniline in its emeraldine salt form, respectively.[49] From Fig. 3(b) and (c), it can be seen that the peaks of polyaniline are substituted by a broad peak indicating that the grain size of PANI has decreased sharply and much more dislocations may occur during the cryogenic grinding process. Meanwhile, the XRD peaks from rGO are observed at 2θ=25.4°, indicating the successful reduction of GO.[50] No obvious PANI peaks but obvious rGO are observed

in the XRD pattern for the PANI/rGO composites. This could be attributed to two possible reasons. One is that the size of PANI/rGO decreases sharply and the partial amorphization of PANI may occur during CG process. The other is that the surface of rGO has been covered with a large amount of small PANI granules.

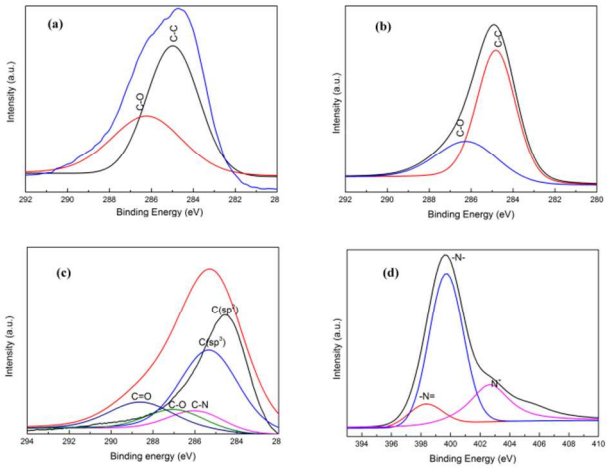

Fig.4 –C 1s XPS spectra of (a) GO, (b) rGO， (c) PANI，and (d) N 1s XPS spectra of CGed-(5%wt.)rGO/PANI.

Table 1 Elemental composite of (a), (b), (c) and (d)

	C	O	N
(a)PANI	80.25%	10.04%	6.44%
(b)GO	64.56%	30.28%	--------
(c)rGO	89.22%	7.27%	--------
(d)CGed(5%wt.)rGO/PANI	88.26%	7.00%	3.32%

The XPS spectra of GO, rGO and CGed-rGO(5%wt.)/PANI are shown in Fig.4. The core-level XPS signal of C 1s for GO and rGO exhibit a main peak centered at about 284.6eV originating from the graphitic sp2 carbon atoms. The weak peaks located at 286.4eV are due to carbon atoms connecting with oxygenate groups, such as C-O and C=O.[31,39] Meanwhile, as is shown, the peak at 284.6eV of rGO is much taller than the peak of GO and the peak at 286.4eV of GO much fatter than the peak of rGO.[32] GO has a strong oxgen peak representing an oxgen atomic content about 30.28%, higher than that in the rGO (7.27%). As shown in Figure 4d, the C 1s core-level spectrum of as–synthesized rGO-PANI composites can be curve-fitted into five peak components: carbon sp2 at 284.6eV, carbon sp3 at 285.3eV, C-N group at 285.9eV, C-O group at 287.0eV and C=O group at 288.5eV, implying that the C=O groups of reduced graphene oxide were doped into PANI.[45] The interaction between the PANI backbone and reduced graphene oxide sheets results in the increased conjugation and shift in binding energy. The N1s core-level spectrum of as-synthesized rGO/PANI composites can be curve-fitted into three peak components with BEs at 398.2eV, 399.3eV and >400eV, attributable to the amine (-NH-), imine (=N-), and positively charged nitrogen (N+,>400eV) species, respectively.[46] As compared with XPS of PANI, the nitrogen content is decreased in the rGO/PANI composites. All above indicate that rGO doping takes place on the quinoid segment of PANI after cryogenic grinding process.

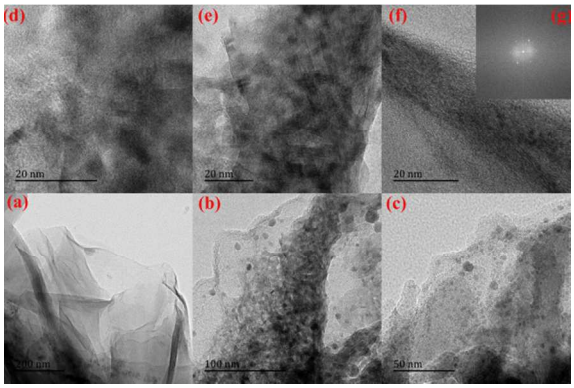

Fig.5. TEM images of (a) rGO and (b-f) the hybrid CGed-PANI/(5%wt.)rGO

The typical morphology of the resulting rGO and the hybrid CGed-PANI/(5%wt.)rGO composites are observed by TEM, as shown in Figure 5. The typical wrinkled layer morphology of the rGO is given in the Figure 5a, which shows the layer-by-layer structure and network structure of rGO. For CGed-PANI/(5%wt.rGO) composite in the Figure 5(b-g), we can see the CGed-PANI are homogeneously dispersed on the rGO sheets. The PANI shows granular and rod-like morphology with 20-60nm. The selected area electron diffraction pattern in inset of Fig.5 (f) shows the PANI lacks obvious crystalline character and the rGO pared here has a typically curved with good crystalline character. All above are because a serious brittle fracturing of the PANI powder could occur in the liquid nitrogen at -195.6 ℃. And grinding is favorable for polymer chain fission, cross-linking and an increase in the amorphous content. We can see that the ordered molecular structure PANI on the surface of reduced grapheme oxide layer after CG progress. TEM images show that the uniform PANI mainly disperses on the surface or intercalates between the rGO sheets because of the strong π–π interaction. The homogeneous dispersion of PANI on rGO sheet indicates that the cryogenic grinding is a simple, effective and low-cost method.

Thermoelectric properties

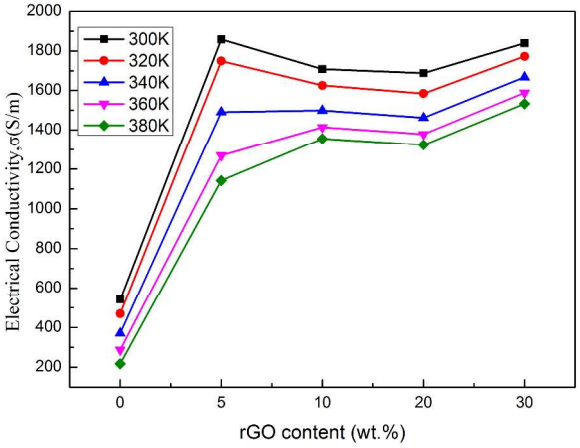

(a)

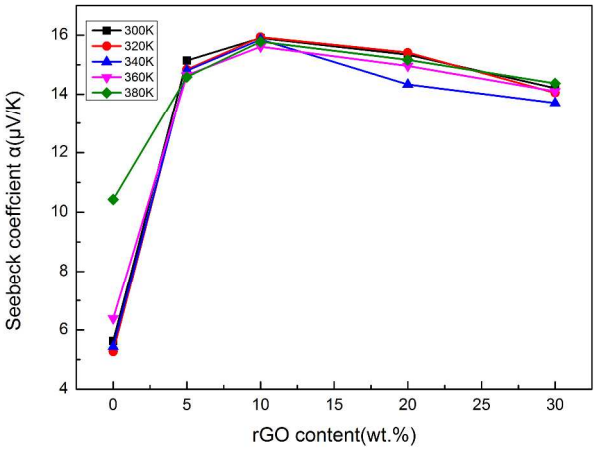

(d)

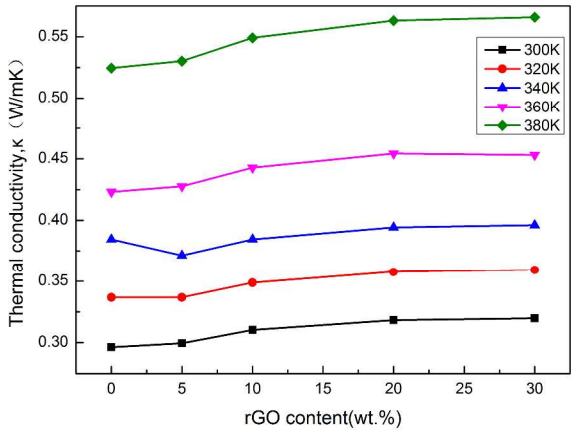

(b)

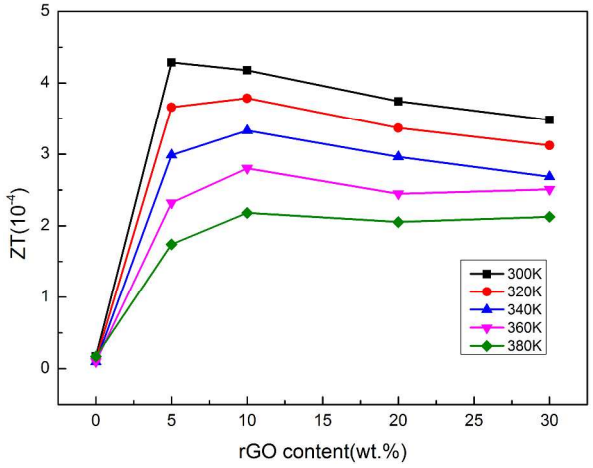

(e)

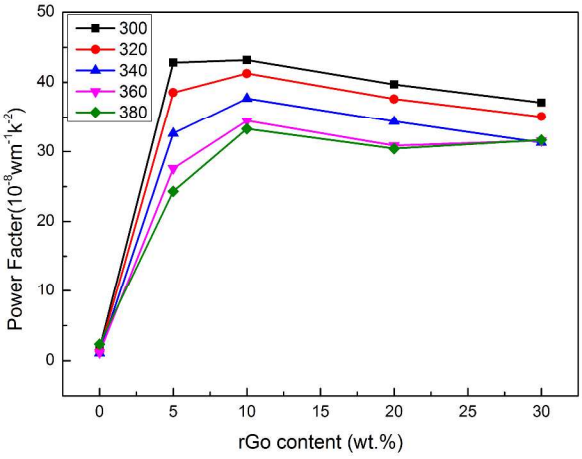

(c)

Fig.6 The electrical conductivity (a), the Seebeck coefficient (b), the power factor (c), the thermal conductivity values (d) and the ZT value (e) of rGO/PANI hybrid composites with different contents rGO.

Table 2 Carrier concentration and carrier mobility of rGO composites with different rGO contents

Sample	Carrier concentration(cm^{-3})	Carrier mobility(cm^2/Vs)
PANI	$4.9x10^{21}$	0.69
5%rGO/PANI	$9.8x10^{21}$	1.38
10%rGO/PANI	$8.5x10^{21}$	1.09
20%rGO/PANI	$8.9x10^{21}$	1.18
30%rGO/PANI	$7.9x10^{21}$	1.21

The thermoelectric properties of the composites were measured in the temperature ranging from 300K to 380K, as shown in Fig.6 (a-e).It can be seen that the electrical conductivity of the composites increases dramatically as the rGO content increases, and reaches 1868.8 S/m for the sample with rGO content of 5% at 300K, which is larger than the pure PANI. The enhancement of the electrical conductivity should be attributed to the strong π-π interaction between π-bonded surface of the rGO and the conjugated structure of polyaniline. This behavior can be explained by the template of reduced graphene oxide created by the rGO and excellent electrical performance of rGO (graphene have high carrier mobility in excess of 10^5 cm^2/Vs , high thermal conductivity up to 5000W/mK and high electrical conductivity about 10^6 S/m).[19,20] Furthermore, the Seebeck coefficient shows great increase from 5.3 to 15.9 μV/K when the rGO content changes from 0 to 10wt%. The positive Seebeck coefficient indicates that the composite is a P-type semiconductor. The rGO content dependence of the power factor is shown in Fig. 6c. It can be seen that the power factor increases obviously from 1.1×10^{-8} W/mK^2 to 42.8×10^{-8} W/mK^2 with the increase of rGO from 0 to 10%. But both the electrical conductivity and Seebeck coefficient are slightly reduced with rGO content ranging from 5% to 30%. The possible reason may be that the rGO is not reduced absolutely (as shown in the elemental composite (c) of Table 1) and oxygen-containing groups of rGO may hinder the carrier transport. Furthermore, all samples exhibit low thermal conductivity values in the range of 0.296-0.566 W/mK in Fig.6 (d). But the thermal conductivity values of the rGO/composites slightly increase with rGO content ranging from 5% to 30%. RGO sheets have higher thermal conductivity values about (4.84 ± 0.44)-$(5.30\pm0.48)\times10^{-3}$ W/mK than PANI, so the thermal conductivity values of composites increases with rGO content. [51-55]

In order to clarify the reason for the changes in electrical conductivity, we measured the hall coefficient (RH) at room temperature on a PPMS system and calculated the carried concentrations, assuming parabolic bands and a single band conduction process. As shown in Table 2, when the rGO content changes from 0 to 5 wt%, the carrier mobility increases greatly. It is also found that the carrier concentration shows little change with the increase of rGO content. This also plays a major role in the increase of Seebeck coefficient. As is known, interchain and intrachain hopping have important effects on the charge carrier transport in polymers. The carrier mobility is strongly dependent on the conformation and arrangement of polymer chains. After CG process, the size of PANI gets smaller. The rGO becomes a template for conductive PANI and a wonderful conductive medium. This highly oriented polymer chains can reduce the barriers of interchain and intrachain hopping and allow the carrier to move easily.Typically, the electrical conductivity of inorganic semiconductor TE materials rises with the increasing carrier concentration, but on the contrary, the Seebeck coefficient tends to reduce at the same time.[57] However, the Seebeck coefficient of Polymer thermoelectric materials often rises even when the electrical conductivity increases. We can see the same changing trend in some other PANI system, such as PANI/Te composite, PANI/ SWNT, PANI/GO and so on.[58-61] In our work, polyaniline molecules ordered on the rGO surface with the induction of rGO and π - π conjugate effect between the PANI and rGO. So the carrier concentration of composite increased with 5%rGO. However, with more rGO added, the oxygen-containing groups on the surface of the rGO increase the barriers of interchain and intrachain. And some electrons become "cold" electrons whose energy is below the Fermi level of the PANI/rGO composite. So the carrier concentration reduced with more rGO added.[58] So the carrier mobility increases, resulting in increased electrical conductivity.[15,56]

The highest ZT value is 4.29×10^{-5} at 300 K for the 5 wt.% sample. The enhancement of the thermoelectric performance should be attributed to the interaction between PANI and the rGO. Compared with the in situ polymerization method, cryogenic grinding has obvious advantages in improving the degree of dispersion of the rGO. The increased contact area strengthens the conjugation between the rGO and PANI molecules, and lowers the carrier hopping barrier. After CG progress, the PANI particles dispersed on the rGO sheet, increasing the carrier transport as a conducting bridge.

Conclusions

The rGO/PANI composites have been prepared through cryogenic grinding technique combined with Spark Plasma Sintering. The results show that the refined PANI particles are homogeneously dispersed and orderly arranged on the rGO templates, which gives rise to the simultaneous enhancement of carrier concentration and carrier mobility. As the rGO content increases from 0% to 30%, the electrical conductivity of rGO/PANI increase from 217 S/m to 1869 S/m, and the thermal conductivity shows little change. On the other hand, rGO are been uniformly dispersed in the composites after CG process. The rGO has two important roles both as conducting medium and the template. Consequently, the maximum ZT of 4.29×10^{-4} is found at 300 K for the PANI sample with 5 wt% rGO, much higher than that of the PANI without rGO ($ZT=1.73\times10^{-5}$), which suggests the superiority of CG technique on the dispersion of PANI and the high efficiency of rGO on enhancing thermoelectric properties. These results demonstrate that the addition of rGO by cryogenic grinding is an effective way for improving the thermoelectric properties of PANI, which could be applicable to many other thermoelectric materials. Finally, As for bulk materials, the ZT value of 4.29×10^{-4} is not very well Compared with film materilas. Nevertheless, bulk materials are more conducive to prepare thermoelectric devices with various shapes. So it is expected to further improve the thermoelectric performance through further optimization of doping level and the microstructure of polyanilin.[56] Meanwhile, the ZT of our composite are still not too high. So it is necessary to improve the degree of order of polyaniline polymer to enhance ZT.

Acknowledgements

This work was funded by Natural Science Foundation of China (No. 51374078 and 51403037), Shanghai Committee of Science and Technology (No. 13JC1400100), "Shu Guang" project supported by Shanghai Municipal Education Commission and Shanghai Education Development Foundation (No.11SG34), PCSIRT (No.IRT1221), the Fundamental Research Funds for the Central Universities and DHU Distinguished Young Professor Program in University.

References

1. Lyeo H-K, Khajetoorians A, Shi L, Pipe KP, Ram RJ, Shakouri A, et al. *Science*. **2004**;303(5659):816-8.
2. Minnich A, Dresselhaus M, Ren Z, Chen G. *Energy & Environmental Science*. **2009**;2(5):466-79.
3. Nolas GS, Sharp J, Goldsmid HJ. *Springer*. **2001**.
4. Heremans JP, Jovovic V, Toberer ES, Saramat A, Kurosaki K, Charoenphakdee A, et al. *Science*. **2008**;321(5888):554-7.
5. Min Y, Roh JW, Yang H, Park M, Kim SI, Hwang S, et al. *Advanced Materials*. **2013**;25(10):1425-9.
6. Zhang Q, Ai X, Wang W, Wang L, Jiang W. *Acta Materialia*. **2014**;73:37-47.
7. Toprak MS, Stiewe C, Platzek D, Williams S, Bertini L, Muller EC, et al. *Advanced Functional Materials.* **2004**;14(12):1189-96.
8. Zhao L-D, Lo S-H, Zhang Y, Sun H, Tan G, Uher C, et al. *Nature*. **2014**;508(7496):373-7.
9. Bubnova O, Khan ZU, Malti A, Braun S, Fahlman M, Berggren M, et al. *Nature materials*. **2011**;10(6):429-33.
10. Yoon C, Reghu M, Moses D, Heeger A, Cao Y, Chen T-A, et al. *Synthetic metals*. **1995**;75(3):229-39.
11. Yakuphanoglu F, Senkal B. *The Journal of Physical Chemistry C*. **2007**;111 (4):1840-6.
12. Du Y, Shen SZ, Cai K, Casey PS. *Progress in Polymer Science*. **2012**;37(6):820-41.
13. Yakuphanoglu F, Senkal BF. *Journal of Physical Chemistry C*. **2007**;111(4):1840-6.
14. Wu CG, DeGroot DC, Marcy HO, Schindler JL, Kannewurf CR, Liu YJ, et al. *Chemistry of Materials*. **1996**;8(8):1992-2004.
15. Zhao Y, Tang G-S, Yu Z-Z, Qi J-S. *Carbon*. **2012**;50(8):3064-73.
16. Zhang Q, Wang W, Li J, Zhu J, Wang L, Zhu M, et al. *Journal of Materials Chemistry A*. **2013**;1(39):12109-14.
17. Qun W, Qin Y, Jiang C, Lidong C. *Journal of Materials Chemistry*. **2012**;22(34):17612-18.
18. Xiang J, Drzal LT. *Polymer*. **2012**;53(19):4202-10.
19. Novoselov KS, Geim AK, Morozov S, Jiang D, Zhang Y, Dubonos S, et al. *science*. **2004**;306(5696):666-9.
20. Geim AK, Novoselov KS. *Nature materials.* **2007**;6(3):183-91.
21. Bunch JS, van der Zande AM, Verbridge SS, Frank IW, Tanenbaum DM, Parpia JM, et al. *Science*. **2007**;315(5811):490-3.
22. Lightcap IV, Kosel TH, Kamat PV.*Nano Letters*. **2010**;10(2):577-83.
23. Eda G, Fanchini G, Chhowalla M. *Nature Nanotechnology*. **2008**;3(5):270-4.
24. Tapaszto L, Dobrik G, Lambin P, Biro LP. *Nature Nanotechnology*. **2008**;3(7):397-401.
25. Zhu Y, Murali S, Stoller MD, Ganesh KJ, Cai W, Ferreira PJ, et al. *Science*. **2011**;332(6037):1537-41.
26. Yoo E, Kim J, Hosono E, Zhou H-s, Kudo T, Honma I. *Nano Letters.* **2008**;8(8):2277-82.
27. Wang X, Zhi L, Muellen K. *Nano Letters*. **2008**;8(1):323-7.
28. Kim M, Lee C, Jang J. *Advanced Functional Materials*. **2014**;24(17):2489-99.
29. Neto AC, Guinea F, Peres N, Novoselov KS, Geim AK. *Reviews of modern physics*. **2009**;81(1):109.
30. Wu Q, Xu Y, Yao Z, Liu A, Shi G. *Acs Nano.* **2010**;4(4):1963-70.
31. Zhang K, Zhang LL, Zhao XS, Wu J. *Chemistry of Materials*. **2010**;22(4):1392-401.
32. Kumar NA, Choi H-J, Shin YR, Chang DW, Dai L, Baek J-B. *ACS nano.* **2012**;6(2):1715-23.
33. Al-Mashat L, Shin K, Kalantar-Zadeh K, Plessis JD, Han SH, Kojima RW, et al. *The Journal of Physical Chemistry C*. **2010**;114(39):16168-73.
34. Huang J, Moore JA, Acquaye JH, Kaner RB. *Macromolecules*. **2005**;38(2):317-21.
35. Long Y, Chen Z, Zhang X, Zhang J, Liu Z. *Applied physics letters*. **2004**;85(10):1796-8
36. MacDiarmid AG, Epstein AJ. *Synthetic Metals.* **1995**;69(1):85-92.
37. Park S, An J, Piner RD, Jung I, Yang D, Velamakanni A, et al. *Chemistry of Materials*. **2008**;20(21):6592-4.
38. Gao W, Alemany LB, Ci L, Ajayan PM. *Nature Chemistry*. **2009**;1(5):403-8.
39. Botas C, Álvarez P, Blanco P, Granda M, Blanco C, Santamaría R, et al. *Carbon*. **2013**;65:156-64.
40. Yu P, Li Y, Zhao X, Wu L, Zhang Q. *Langmuir.* **2014**;30(18):5306-13.
41. Lindfors T, Latonen R-M. *Carbon*. **2014**;69:122-31.
42. Yan J, Wei T, Shao B, Fan Z, Qian W, Zhang M, et al. *Carbon.* **2010**;48(2):487-93.
43. Valles C, Jimenez P, Munoz E, Benito AM, Maser WK. *Journal of Physical Chemistry C.* **2011**;115(21):10468-74.
44. Huang X, Hu N, Gao R, Yu Y, Wang Y, Yang Z, et al. *Journal of Materials Chemistry.* **2012**; 22(42):22488-95.
45. Mi L, Xingyi H, Chao W, Haiping X, Pingkai J, Tanaka T. *Journal of Materials Chemistry.* **2012**;22(44):23477-84.
46. Lu J, Liu W, Ling H, Kong J, Ding G, Zhou D, et al. *Rsc Advances.* **2012**;2(28):10537-43.
47. Liu P, Huang Y, Wang L, Zhang W. *Synthetic Metals.* **2013**;177:89-93.
48. Kumar NA, Choi H-J, Shin YR, Chang DW, Dai L, Baek J-B. *Acs Nano.* **2012**;6(2):1715-23.
49. Wang W, Sun S, Gu S, Shen H, Zhang Q, Zhu J, et al. *RSC Advances*. **2014**. **4** (51), 26810-26816 .
50. Wang H, Hao Q, Yang X, Lu L, Wang X. *Nanoscale.* **2010**;2(10):2164-70.
51. Seol JH, Jo I, Moore AL, Lindsay L, Aitken ZH, Pettes MT, et al. *Science*. **2010**;328 (5975):213-6.
52. H. Yan, T. Ohta and N. Toshima, *Macromolecular Materials and Engineering.* **2001**, 286, 139-142.
53. H. Yan, N. Sada and N. Toshima, *Journal of Thermal Analysis and Calorimetry*. **2002**, 69, 881-887.
54. R. Islam, R. Chan-Yu-King, J.-F. Brun, C. Gors, A. Addad, M. Depriester, A. Hadj-Sahraoui and F. Roussel, *Nanotechnology* .**2014**, 25, 475705.
55. J. Choi, N. D. Tu, S.-S. Lee, H. Lee, J. S. Kim and H. Kim, *Macromolecular Research*. **2014**, 22, 1104-1108.
56. Q. Yao, L. Chen, W. Zhang, S. Liufu and X. Chen, *Acs Nano.* **2010**, 4, 2445-2451.
57. D. M. Rowe, CRC handbook of thermoelectrics, CRC press, **1995**, p.
58. N. E. Coates, S. K. Yee, B. McCulloch, K. C. See, A. Majumdar, R. A. Segalman and J. J. Urban, *Advanced Materials*

2013, 25, 1629-1633.
59. Q. Yao, Q. Wang, L. Wang, Y. Wang, J. Sun, H. Zeng, Z. Jin, X. Huang and L. Chen, *Journal of Materials Chemistry A* **2014**, 2, 2634-2640.
60.Q. Yao, Q. Wang, L. Wang and L. Chen, *Energy & Environmental Science* **2014**, 7, 3801-3807.
61. Y. Zhao, G.-S. Tang, Z.-Z. Yu and J.-S. Qi, *Carbon* **2012**, 50, 3064-3073.